Cost-Effective Metasurface-Enabled Microstrip Antennas for Dual-band mmWave Applications in 5G Networks

Nuttaphat Prasert[1], Chawalit Rakluea[2], and Sarawuth Chaimool[1,a]
[1]*Electrical Engineering, Khon Kean University, Khon Kaen, Thailand,* [a]ORCID: 0000-0002-2412-2921
[2]*Electronics and Telecomunication Engineering, Rajamangala University of Technology Thanyaburi, Pathum Thani, Thailand*

***Abstract*— This paper proposes a cost-effective design approach for metasurface-enabled microstrip antennas optimized for the dual-band of mmWave 5G frequencies, specifically 26 GHz (n258) and 28 GHz (n257). The proposed antennas are based on metasurface and are manufactured using standard printed circuit board (PCB) processes on a low-cost FR-4 substrate, making them suitable for mass production at an affordable price. The dimensions of the proposed antenna are 25×25×7.6 mm³ . It demonstrates a $|S_{11}| \leq$ -10 dB bandwidth of 31.9% (23.2-32.0 GHz) and offers a higher gain of 7.2 dB compared to a non-metasurface patch antenna with a gain of 5.12 dBi. The proposed antenna achieves a peak gain of 13.8 dBi and maintains a good front-to-back ratio exceeding 15 dB across the entire operating band. Moreover, the use of low-cost FR-4 substrate and PCB fabrication processes ensures cost-effectiveness, making these antennas highly suitable for cost-efficient deployment in 5G applications.**

Keywords—FR-4, low-cost, wideband, millimeter, NR, planar antenna

I. Introduction

The demand for high-speed and high-capacity wireless communication systems has been rapidly increasing with the advent of fifth-generation (5G) networks. Millimeter-wave (mmWave) frequencies have emerged as a promising solution for 5G networks due to their abundant available bandwidth. However, designing efficient and wideband antennas for mmWave applications while keeping the cost low remains a significant challenge. While there are various reported approaches for designing planar millimeter-wave antennas, all of them utilize commercially available low-loss substrates, specifically Rogers RT/duroid substrates, with a loss tangent of less than 0.0027 [1]-[4]. Moreover, advanced antenna materials, such as Low Temperature Co-fired Ceramics (LTCC)[5], PTFE [6], or organic PCBs like Liquid Crystal Polymer (LCP) [7], are utilized in the design of millimeter-wave antennas. Nonetheless, these materials are either excessively expensive or require a complicated manufacturing process. The challenge in achieving mass production of millimeter-wave applications lies in the high cost or complex manufacturing process of the available materials. One possible solution to this challenge is to design low-cost millimeter-wave antennas. FR-4 is a low-cost and readily available substrate material, making it an attractive choice for mass production of antennas, which are widely used in commercial printed circuit boards (PCBs). By incorporating metasurfaces with microstrip antennas on FR-4 substrates, it is possible to enhance the antenna performance in terms of bandwidth, gain, and radiation efficiency, while keeping the costs low. Despite the growing demand for low-cost mmWave antennas on FR-4 substrates for 5G networks, there are still several gaps in the current research and development. Some of the main challenges in this area revolve around the high substrate loss associated with FR-4 substrates, the lack of standardization in design guidelines, and the limited experimental validation of FR-4-based mmWave antennas [8]-[9]. In recent years, metasurfaces have gained significant attention as a promising technology for enhancing the performance of antennas [10]-[12]. Metasurfaces are subwavelength structures that manipulate the properties of electromagnetic waves, enabling control over the direction, polarization, and phase of the radiated fields.

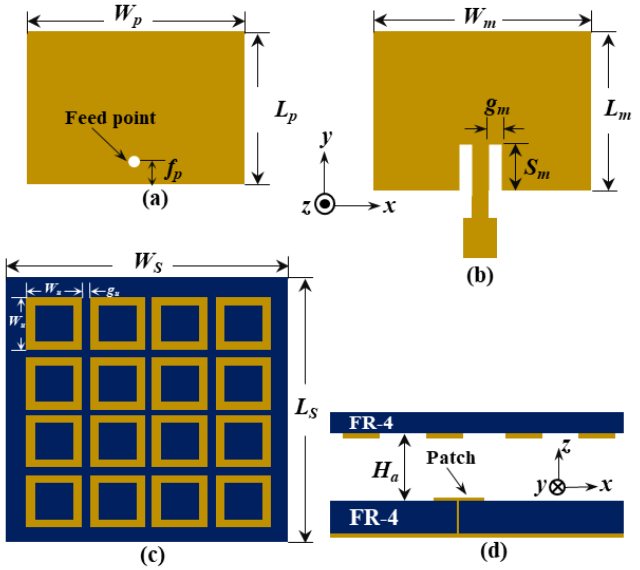

Fig. 1. The configuration of the proposed antenna (a) probe feed (b) microstrip feed with inset feed (c) metasurface and (d) the proposed antenna structure.

By carefully engineering the geometry and arrangement of subwavelength resonant elements (unit cells) on the metasurface, it is possible to control the amplitude, phase, and polarization of the transmitted and reflected waves. In the case of an antenna using FR-4 substrate, which has a high loss tangent, the metasurface can be utilized to compensate for the substrate's lossy behavior. Specifically, the metasurface can be designed to enhance the radiation efficiency of the antenna by providing additional degrees of freedom to shape the radiated fields.

This paper proposes metasurface-based microstrip antenna for use in the dual-band of mmWave 5G frequencies of 26 GHz and 28 GHz. The proposed antenna and metasurface are designed to be cost-effective, utilizing a single FR-4 substrate. Prototypes have been fabricated and experimentally measured, with the results showing good agreement with the simulated performance.

II. Antenna Geometry and Design Considerations

The configuration of the proposed antenna is demonstrated in Fig. 1. The antenna comprises a driven microstrip patch beneath a metasurface. Two excitation antennas have been designed for comparison, namely a probe feed and a microstrip feed as shown in Fig. 1(a) and (b), respectively. The MTS (Fig. 1 (c)) consists of a 4×4 array of square loop resonators (SLRs) and is placed above the driven antenna with H_a as shown in Fig. 1(d). The unit cell of the MTS has a square periodicity of W_g = 2.58 mm, with each loop having a width of 0.6 mm and a gap between loops of 0.6 mm. The driven antenna and MTS are printed on a substrate made of FR-4 with a dielectric constant of 4.5, a thickness of 0.8 mm, and a loss tangent (tan δ) of 0.025.

Our first step is to ascertain the suitable driver for the MTS-based antenna. Figure 2 shows the impacts of the probe feed and microstrip feed in order to choose an appropriate driven antenna. The results indicate that the probe-fed antenna exhibits a broader bandwidth of 14.61%, ranging from 23.91 to 31.66 GHz. On the other hand, although the microstrip feed excites two resonant modes, it has a narrower bandwidth of only 7.41% (24.02-27.96 GHz). Moreover, the probe feed has a higher and flat gain of 4.9 to 5.2 dBi, which can be attributed to its higher radiation efficiency. As a result, the probe feed is chosen as the driven antenna.

Subsequently, a MTS is designed to take the form of a Fabry-Perot cavity (FPC) antenna, which is intended to improve the antenna gain. As per the guidelines outlined in reference [13], to trade-off between the gain and bandwidth the separation distance between the driver and the MTS should be about $0.5\lambda_0$ at 26 GHz. The optimized value of various parameters of proposed structure is as follow: W_S = 25; L_S = 25; H_a = 5.9; W_p = 3.1; L_p = 2.2; f_p = 0.5; W_m = 3.4; L_m = 2.3; S_m = 0.7; g_m = 0.2 (units = mm). The total dimension of the fabricated prototype is found to be 25×25×7.6 mm^3.

III. Results and Discussion

The proposed antenna is analyzed using the CST software, and experiments are carried out using an Agilent 8363B vector network analyzer. In Fig.2, there are two resonances observed in the MTS-based antenna, while the driven probe-fed patch without MTS exhibits only a single resonance. The first resonance, occurring around 24 GHz, is associated with the FPC resonance. This resonance is generated by the multiple reflections within the cavity, which leads to an increase in the antenna's directivity in the boresight direction [14]. The second resonance at 26 GHz is attributed to the microstrip patch resonance as the primary source. Despite this, both the probe-fed antennas with and without MTS exhibit a similar impedance bandwidth of approximately 14%. The patch antenna with the MTS achieves a peak realized gain of approximately 13.8 dBi. This represents a noticeable improvement over the patch antenna's standalone performance, which achieves only 5.12 dBi gain at 24.5 GHz. Figure 3 illustrates the changes in the magnitude of the S_{11} and

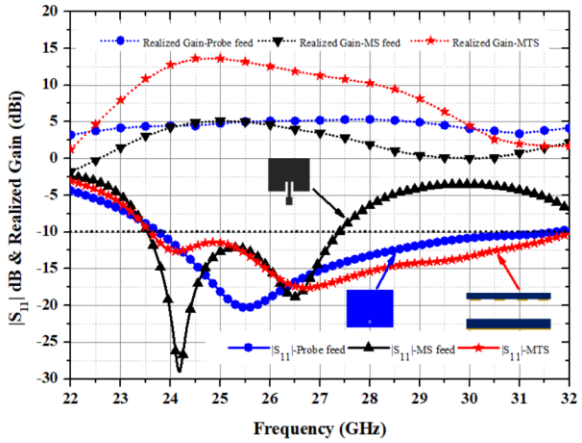

Fig. 2. Simulated $|S_{11}|$ and realized gain of the driven patch antenna with probe feed and microstrip feed.

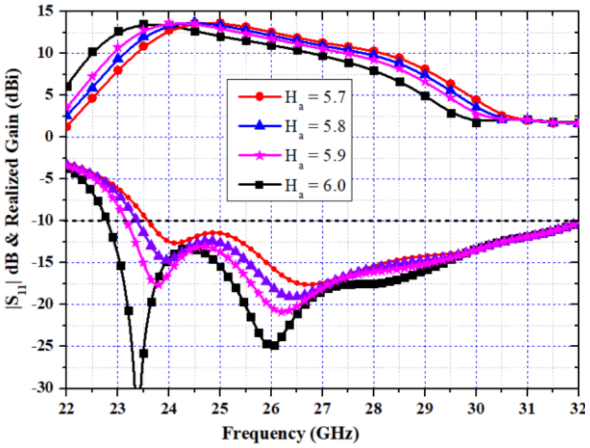

Fig. 3. Variation of |S11| and realized gain when varying the cavity height (H_a).

realized gains of the antenna as the height of the resonant cavity (H_a) is varied. The results indicate that increasing H_a causes the resonant frequency and peak gain to shift towards lower values, while the end of the bandwidth remains constant at 32 GHz. At a resonant cavity height (H_a) of 6.0, the antenna achieves its maximum bandwidth, which spans from 22.8 GHz to 32 GHz, corresponding to a bandwidth of 9.2 GHz or 33.5%.

Figure 4 displays the simulated far-field characteristics of the three antennas at 26 GHz as mentioned in Fig. 2. The results indicate that the radiation patterns of all antennas in the *xz*-plane exhibit broadside directionality. However, in the absence of the MTS, the radiation patterns in the *yz*-plane are directed off-broadside, as depicted in Figure 4(b). These findings suggest that the MTS-formed cavity is capable of adjusting the radiation pattern from off-broadside to broadside. A narrower beamwidth in the MTS-based antenna indicates a higher gain than other antennas. Furthermore, the MTS-based antenna exhibits a side lobe level that is 12 dB lower compared to the antenna without the MTS.

To validate the accuracy of the simulation results, a prototype of the antenna was fabricated and subsequently measured. Figures 5(a) and 5(b) depict the photograph of the fabricated antenna structure and the set-up for the measurement of radiation pattern in anechoic chamber, respectively. The probe-fed patch antenna and MTS were

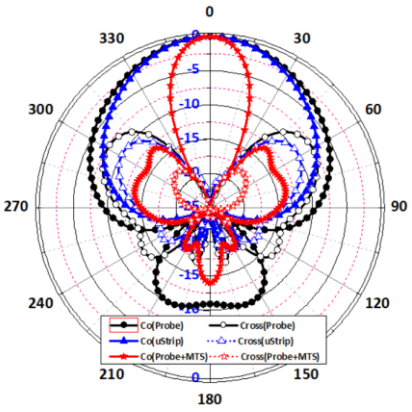

(a)

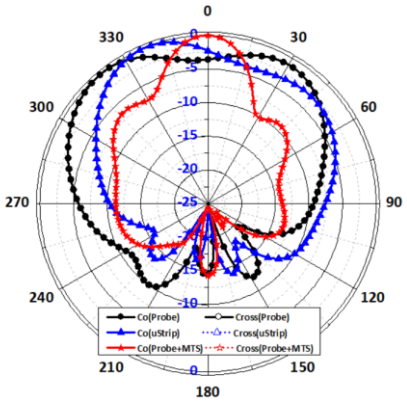

(b)

Fig. 4. Simulated radiation patterns at 26 GHz (a) *xz*-plane and (b) *yz*-plane.

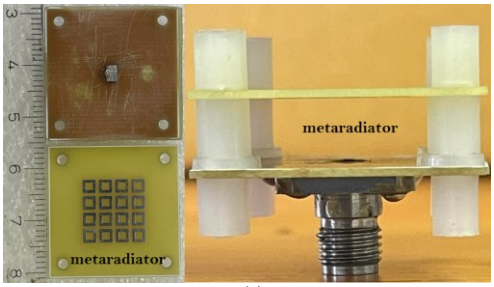

(a)

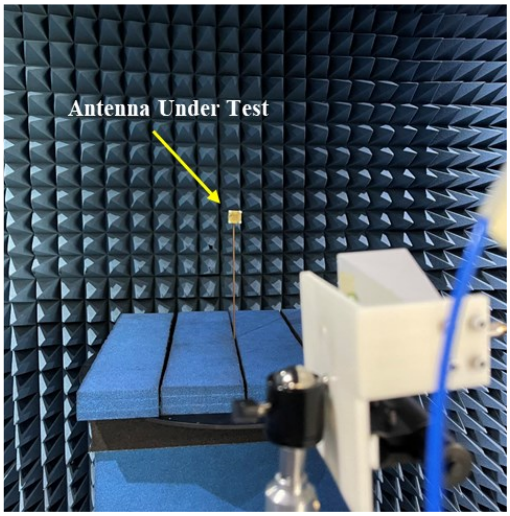

(b)

Fig. 5. Photograph of a antenna prototype and (b) the measurement set-up in anechoic chamber.

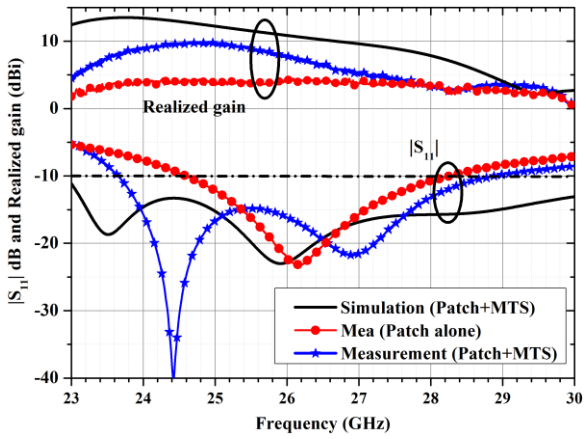

Fig. 6 Comparison of $|S_{11}|$ and realized gains between a antenna with the MTS and a patch-alone based on both measurement and simulation results with a good matching when H_a = 5.9 mm.

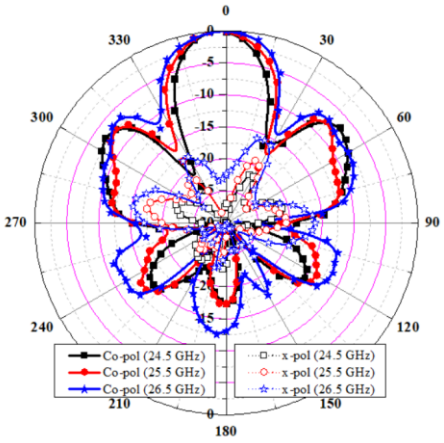

(a)

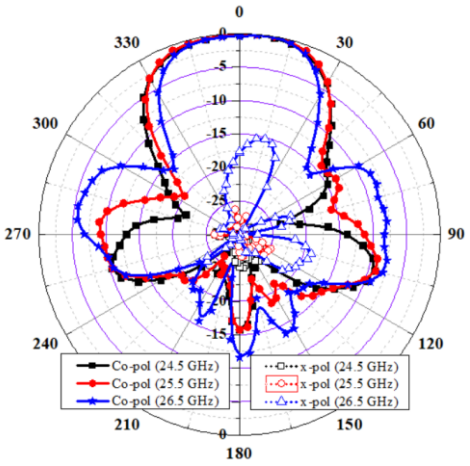

(b)

Fig. 7. Measured radiation pattern with three frequecnies of 24.5, 25.5 and 26.5 GHz (a) *xz*-plane and (b) *yz*-plane

fabricated using low-cost FR-4 with industrial electronic PCB processing with a processing tolerance of 0.1 mm. Figure 6 illustrates a comparison of the $|S_{11}|$ and realized gains between a well-matched MPA with the MTS and a well-matched MPA-alone based on both measurement and simulation results. Observing the results, it becomes apparent that the patch in isolation exhibits just one resonance occurring at 26.2 GHz. However, when the patch is combined with the MTS, it

manifests two resonances. The resonances determined through simulation are situated at 23.5 GHz and 25.9 GHz, whereas the resonances obtained through measurement are slightly shifted to higher frequencies, specifically 24.4 GHz and 26.9 GHz. The measured bandwidth, ranging from 23.64 GHz to 28.88 GHz, accounts for a narrower range of 20% compared to the simulated bandwidth. The simulated bandwidth covers a larger span from 22 GHz to 30 GHz, aligning with the 5G FR2 bands at 26 GHz (n258) and 28 GHz (n257). These discrepancies between the measured and simulated results may be due to the antenna's sensitivity to changes in the cavity height (H_a), which can be affected by errors in alignment during fabrication. Additionally, the simulation does not consider the SMK port for probe feed. Furthermore, the comparison between the patch-alone and the patch with the MTS extends to the realized gains. It is evident that the patch with the MTS exhibits a higher gain compared to the patch alone, with an increase of approximately 7.2 dB, increasing from 4.1 dBi to 11.3 dBi. However, it should be noted that the measured gain is slightly lower than the simulated gain.

The radiation patterns in two principal planes were measured and are depicted in Figure 7. The patterns demonstrate excellent broadside radiation and a cross-polarization less than -18 dB, particularly in the *xz*- plane. Additionally, the front-to-back ratios (FBR) were measured and found to exceed 12 dB across all operating frequencies. However, both sidelobe, cross polarization and FBR levels increase as frequency increases.

IV. Conclusion

Cost-effective metasurface-enabled microstrip patch antennas on FR-4 substrates hold tremendous potential for wideband mmWave applications in 5G networks. Although FR-4 substrates are low-cost and readily available, they may exhibit lower gain and efficiency than low-loss substrates. However, integrating metasurfaces has demonstrated improvements in the gain-bandwidth performance of microstrip antennas on FR-4 substrates. The proposed antenna design aims to leverage the benefits of metasurface integration to enhance antenna performance while addressing cost-effectiveness. These antennas offer affordability, dual-band operation, and improved gain-bandwidth, making them highly promising for wideband mmWave applications in 5G networks. By customizing the metasurface to the specific antenna and substrate properties, it is possible to improve antenna gain and efficiency while reducing the substrate's lossy behavior. This can result in enhanced overall antenna performance and superior communication system performance.

Acknowledgment

The authors would like to thank the Wireless Communication Laboratory at the Rajamangala University of Technology Thanyaburi (RMUTT), for the assistance in the radiation pattern and gain measurement.

References

[1] M. Khalily, R. Tafazolli, T. A. Rahman and M. R. Kamarudin, “Design of phased arrays of series-fed patch antennas with reduced number of the controllers for 28-GHz mm-wave applications,” IEEE Antenna Wirel. Propag. Lett., vol. 15, pp. 1305-1308, 2016.

[2] W. A. Awan, M. Alibakhshikenari and E. Limiti, “High gain dual parasitic patch loaded wideband antenna for 28 GHz 5G applications,” in *Proc*. Int. Symp. Antennas Propag., Taiwan, 2021, pp. 1-2.

[3] Y. He, M. Rao, Y. Liu, G. Jing, M. Xi and L. Zhao, “28/39-GHz dual-band dual-polarized millimeter wave stacked patch antenna array for 5G applications,” in *Proc.* Int. Workshop Antenna Tech., Romania, 2020, pp. 1-4.

[4] U. Ullah, M. Al-Hasan, S. Koziel and I. B. Mabrouk, “A series inclined slot-fed circularly polarized antenna for 5G 28 GHz applications,” IEEE Antennas Wirel. Propag. Lett., vol. 20, no. 3, pp. 351-355, March 2021.

[5] H. -T. Chou, S. -J. Chou, J. D. S. Deng, C. -H. Chang and Z. -D. Yan, “LTCC-based antenna-in-package array for 5g user equipment with dual-polarized endfire radiations at millimeter-wave frequencies,” IEEE Trans. Antennas Propag., vol. 70, no. 4, pp. 3076-3081, April 2022.

[6] W. Kim, J. Bang and J. Choi, “A cost-effective antenna-in-package design with a 4 × 4 dual-polarized high isolation patch array for 5G mmWave applications,” IEEE Access, vol. 9, pp. 163882-163892, 2021.

[7] I. -J. Hwang, J. -I. Oh, H. -W. Jo, K. -S. Kim, J. -W. Yu and D. -J. Lee, “28 GHz and 38 GHz dual-band vertically stacked dipole antennas on flexible liquid crystal polymer substrates for millimeter-wave 5G cellular handsets” IEEE Trans. Antennas Propag., vol. 70, no. 5, pp. 3223-3236, May 2022.

[8] X. Liu, W. Zhang, D. Hao and Y. Liu, “Cost effective broadband and compact patch antenna based on ball grid array packaging for 5G NR FR2 band applications,” IEEE Trans. Circuits Sys. II: Express Briefs, doi: 10.1109/TCSII.2022.3233381.

[9] X. Liu, W. Zhang, D. Hao, and Y. Liu, “Differential-fed magneto-electric dipole antenna with integrated balun based on ball grid array packaging,” IEEE Trans. Components, Packaging Manufacturing Technol., pp. 1–1, 2022.

[10] S. Chaimool, C. Rakluea, and P. Akkaraekthalin, "Mu-Near-Zero metasurface for microstrip-fed slot antennas,” Applied Physics A: Vol. 112, no. 3 , pp. 669-675, 2013.

[11] S. Chaimool, C. Rakluea and P. Akkaraekthalin, “Low-profile unidirectional microstrip-fed slot antenna using metasurface,” in *Proc*. Int. Symp. Intell. Signal Processing Commu. Sys., Thailand, 2011, pp. 1-5.

[12] S. Chaimool, K. L. Chung, and P. Akkaraekthalin, “Simultaneous gain and bandwidths enhancement of a single-feed circularly polarized patch antenna using a metamaterial reflective surface,” Prog. In Electromagnetics Research B, Vol. 22, pp. 23-37, 2010.

[13] P. Xie, G. Wang, H. Li and X. Gao, “A novel methodology for gain enhancement of the Fabry-Pérot antenna,” IEEE Access, vol. 7, pp. 176170-176176, 2019.

[14] S. Chaimool, K. L. Chung, and P. Akkaraekthalin, “Bandwidth and gain enhancement of microstrip patch antenna using metamaterial reflective surface,” (invited paper) IEICE Transactions on Communications, vol. E93-B, no.10, pp. 2496-2503, October 2010.